Needle Placement using Patient-Specific, Skew-Line Needle Guides for Prostate HDR Brachytherapy: An Open-Loop Phantom Study

Timmy Siauw and J. Adam Cunha
Radiation Oncology, University of California, San Francisco, San Francisco, CA, USA

Animesh Garg, Sachin Patil, and Ken Goldberg
Industrial Engineering and Operations Research, University of California, Berkeley, Berkeley, CA, USA

I-Chow Hsu and Jean Pouliot
Radiation Oncology, University of California, San Francisco, San Francisco, CA, USA

Abstract

Purpose: Recent advances in real time 3D ultrasound, EM tracking, needle position optimization, and rapid prototyping support a radically new prostate high dose rate (HDR) brachytherapy workflow that uses custom needle guides to insert needles. The purpose of this study is to evaluate one part of this workflow: the needle placement error associated with using a rapidly prototyped (3D printed) needle guide to insert skew-line needle arrangements and the effect this error has on treatment quality.

Method: We created four gelatin phantoms to simulate prostate cancer cases. We used Needle Planning by Integer Program (NPIP) to generate a skew-line needle arrangement for each phantom. A dose distribution was computed for each needle arrangement using Inverse Planning by Integer Program (IPIP). We 3D printed a needle guide to accommodate each needle arrangement and used it to insert the needles into the phantoms. We did not use any feedback or sensing information to alter the trajectory of the needles into a more desirable arrangement. We evaluated the implanted needle arrangements by placement error, critical structure puncturing, and the final dose distribution.

Results: Three phantoms were successfully implanted without puncturing any non-target structure. One case punctured the urethra, and we considered this case a failure. The RMS distance between the planned and implanted needles was 3.6 mm, 3.0 mm, 4.5 mm, and 2.3 mm, respectively. Most of this error was along the needle insertion direction, i.e., z-direction. The RMS distance between the planned and implanted needles was 1.4 mm, 1.7 mm, 1.5 mm, and 0.9 mm, respectively, when only the x- and y-direction error was included. Despite these placement errors, a satisfactory dose distribution for our clinic was achieved for every case. The maximum difference in target coverage between the planned and implanted needle arrangement was 2%.

Conclusion: Without the use of real-time feedback, needle insertion using custom needle guides leads to substantial placement errors. These placement errors do not seem to affect the ability to meet clinical dose objectives. Future work will explore these needle guides in the context of a more complete brachytherapy delivery system.

Keywords: HDR brachytherapy, needle planning, custom needle guides, NPIP, optimization

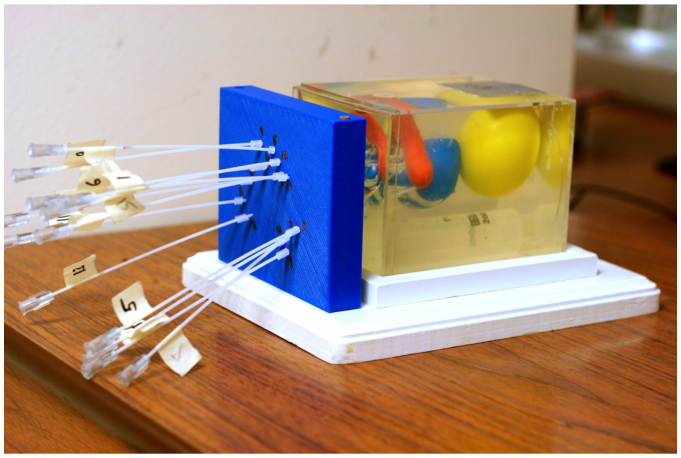

FIG. 1. Recent advances in real time 3D ultrasound, EM tracking, needle position optimization, and rapid prototyping provide the means to radically change the prostate high dose rate (HDR) brachytherapy workflow. In this study, we evaluate the placement errors associated with inserting needles using a custom needle guide for optimized skew-line needle arrangements, which is one part of this workflow. Shown above is a phantom that was implanted using a custom needle guide.

I. INTRODUCTION

High dose rate (HDR) brachytherapy is a radiation therapy for cancer that places a radioactive source in or near the tumor volume using an arrangement of temporarily inserted needles. The dose is delivered to the patient by sequentially threading the radioactive source through each needles, where it can halt at pre-specified dwell positions within the needle. The dose distribution is controlled by altering the dwell time at each dwell position. Studies have shown that HDR brachytherapy is an effective treatment for cancer in the prostate, breast, vagina, cervix, uterus, head, and neck [1–5].

In prostate HDR brachytherapy, the catheters are inserted interstitially through the perineum with the assistance of a rigid needle guide. Although needle guides help maintain a stable trajectory during insertion, they restrict the possible needle arrangements to parallel patterns and offer few opportunities to avoid puncturing organ at risk (OAR) structures such as the neuromuscular bundles near the penile bulb (bulb). Roy et al [6] used custom needle guides to insert non-parallel needle arrangements to help overcome pubic arch interference in prostate permanent-seed implant (PPI) brachytherapy. A few groups have developed freehand, ultrasound-guided, needle insertion techniques that do not require a needle guide

[7]. Freehand techniques allow the physician to adjust the needle trajectories on the fly to improve the final dose distribution and avoid puncturing OAR. However, the effectiveness of freehand techniques is highly skill dependent, and it can take years to master.

Recently there has been a research trend away from parallel needle arrangements in HDR brachytherapy. Foster et al [8] showed that inverse dose planning could compensate for small placement perturbations in needle arrangements. Cunha et al [9] and Xu et al [10] showed that needle arrangements made up of skew-lines (i.e., non-parallel, non-intersecting lines) could achieve brachytherapy dose objectives while avoiding puncturing the bulb. Siauw et al [11] developed Needle Planning by Integer Program (NPIP), which is an inverse planning tool for computing patient-specific, skew-line needle arrangements, and Garg et al [12] showed that a robotic workflow could insert NPIP-generated needle arrangements in a clinical setting with sufficient accuracy to meet dose objectives and avoid puncturing OAR.

Although robot-assisted brachytherapy is a promising framework for performing skew-line, brachytherapy needle insertion, recent advances in 3D ultrasound technology and rapid prototyping allow an alternative framework for this purpose. This framework assumes a clinical environment with real-time, 3D trans-rectal ultrasound [13, 14] , electro-magnetic (EM) needle tracking [15, 16], a rapid prototyping method such as 3D printing or CNC milling/drilling, and an integrated planning system capable of dose planning and needle position planning [11, 17, 18] in addition to the regular brachytherapy delivery infrastructure, i.e., operating room, afterloader, etc. A system with these components could ultrasound scan the patient, design a needle arrangement and custom needle guide, manufacture the guide, and allow the physician to use it to insert the needles. This system would not require the patient to move between rooms to acquire a CT scan. The patient might also benefit from a needle arrangement with fewer needles that avoids puncturing non-target structures while meeting dose objectives, and this needle arrangement could be implanted with the consistency of traditional needle guides and the assistance of EM tracking.

The purpose of this study is to evaluate one part of this framework. Specifically, we evaluate the placement error associated with inserting needles according to a custom needle guide and the effect this error has on the number of structures punctured and the ability to meet treatment objectives. For this study, the needle insertion is performed outside the context of the overall system. Specifically, we do not use any real time feedback to alter the needle arrangement or avoid puncturing non-target structures, and thus the needle insertion

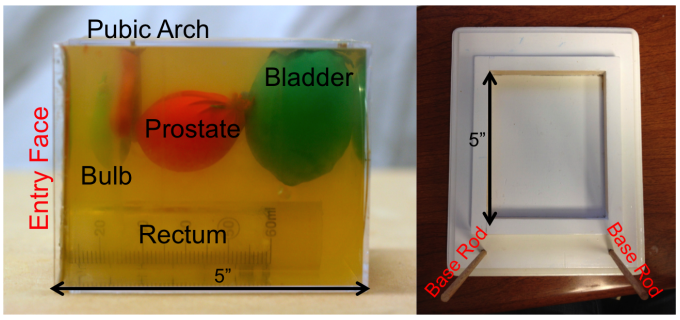

FIG. 2. We performed our needle insertion study on prostate gelatin phantoms (left). The regions of interest included the prostate, urethra, bladder, rectum, penile bulb, and pubic arch. The phantom was registered to the needle guide using a base built specifically for this study (right). The base contained two base rods, which interfaced with the custom needle guide. This figure shows the base from top view.

is open-loop. We perform several placement experiments on prostate gelatin phantoms and discuss implications for the overall workflow. Figure 1 shows our experimental endpoint with a custom needle guide, phantom, and implanted needles.

II. METHOD AND MATERIALS

A. Gelatin Phantoms

Four gelatin phantoms were constructed to simulate human prostate cancer cases. These phantoms cases were labeled C1, C2, C3, and C4, respectively. The anatomical structures included the prostate, urethra, bladder, rectum, penile bulb, and pubic arch. The prostate, bladder, and penile bulb were made from small, latex water balloons filled with a water-milk, gelatin mixture. A plastic drinking straw segment was inserted into the prostate balloon to simulate the urethra length within the prostate. The pubic arch was constructed from clay, which was not puncturable by our needles. The rectum was simulated by a 1 inch (2.5 cm) diameter plastic tube. The phantom was housed in a 4 in $\times$ 4 in $\times$ 5 in (10 cm $\times$ 10 cm $\times$ 12 cm) acrylic box. The anatomical structures were supported by a water, gelatin matrix that had a strong CT contrast to the mixture used for the prostate, bladder, and penile bulb. Figure 2 (left) shows a phantom used in this study. The relevant components and

measurements are labeled.

The contoured prostate volumes for each phantom were 27 cm^3, 26 cm^3, 31 cm^3, and 32 cm^3, respectively.

B. Phantom Registration

A base was constructed to register the phantom to the planning system and the customized guide (Figure 2 (right)). The base was constructed out of wood, which did not produce CT artifacts that could interfere with structure identification and segmentation. The base was designed such that the insertion face of the phantom and the needle guide would be parallel and 2 cm apart. The phantom was immobilized by side supports that were tight to the outer housing of the phantom. The base was designed to hold a rectangular needle guide measuring 12 cm wide $\times$ 10 cm tall $\times$ 2 cm thick. The guide was immobilized by two rods that were perpendicular to the base and 11 cm apart. These rods were constructed from 3/8 in. (4.8 mm) wooden dowels embedded into the base. Each shaft had an associated mating hole in the designed guide.

C. Needle and Dose Optimization

The phantom was placed into the base and scanned using a spiral CT in 3 mm thick slices. The anatomical structures manually segmented in Oncentra v4.3. No margins were added to any of the structures. The base and the phantom housing were also segmented to help register the phantom with the planning system.

A needle arrangement was computed for each anatomical structure set using Needle Planning by Integer Program (NPIP) [11]. Given a set of anatomical structures, NPIP computes the smallest needle arrangement (fewest needles) such that every voxel within the target is within a user-specified distance, δ, from at least one needle in the arrangement. NPIP guarantees that the needles in the arrangement do not come within a distance, γ, from each other (i.e., collision free) and do not puncture any non-target structures. For this study, the γ parameter was set to 4 mm, which was twice the diameter of the needles used in this experiment. In addition to the anatomical structures and δ and γ parameters, NPIP requires an entry zone definition, i.e., convex polygon, through which needles can be inserted

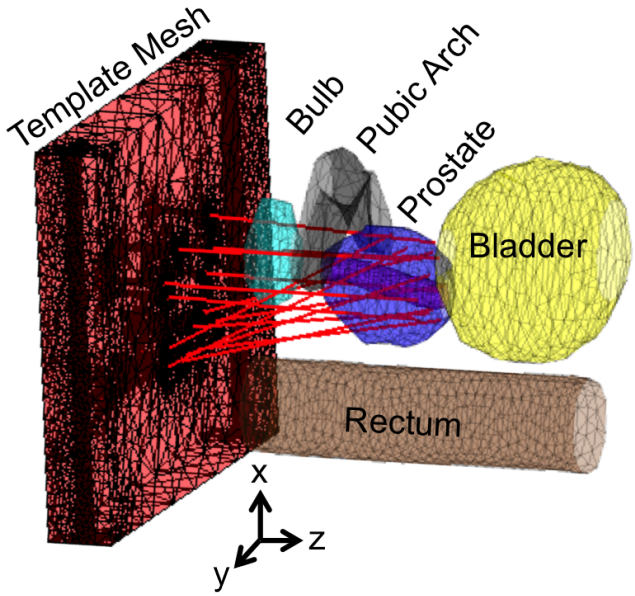

FIG. 3. We computed a planned needle arrangement (red lines) using Needle Planning by Integer Program (NPIP). NPIP is an algorithm for computing custom skew-line needle arrangements that avoid puncturing non-target structures while covering the entire prostate region. A needle guide mesh for the computed needle guide was then computed (red mesh). The coordinate axis convention is also shown.

into the body. In practice, the entry zone for needles is on the surface of the perineum. Since the perineum was not modeled in our phantoms, the entry zone was taken to be a 6 $\times$ 6 cm square, perpendicular to the z-axis, centered at the center of mass of the contoured housing of the phantom. By design, this entry zone was expected to be at the back face of the guide, and smaller than the working area of the phantom, which was 10 $\times$ 10 cm. In practice, the entry zone is most restricted by the pubic arch. Specifically, needles must be inserted at a location and trajectory such that they will avoid the pubic arch. Since the pubic arch was a contoured structure in this study, the location of the entry zone did not need to be restricted by the structure geometry, only the guide geometry.

The final NPIP needle arrangement is selected from a candidate needle set - a large, randomly generated set of skew-line (i.e., non-parallel, non-intersecting) segments that originate from the entry zone. For this study, the initial number of needles generated for the candidate needle set was 5000. Candidate needles that do not intersect the prostate, or

intersect an OAR before intersecting the prostate, are removed from the candidate needle set. The remaining needles are truncated to the last (most superior) dwell position within the prostate, or the last dwell position in the prostate before intersecting an OAR. For this study, the δ parameter was initially set to 32.5% of the prostate radius, which was defined to be the radius of a sphere with equivalent volume to the prostate. This selection of δ usually produces needle arrangements with approximately 14-16 needles [11], where 16 needles is the standard number of needles used at our clinic for HDR brachytherapy. The δ parameter was adjusted from this value as needed to produce a dose plan that met dose objectives.

In NPIP, the final needle arrangement is evaluated by computing a dose plan for it using Inverse Planning by Integer Program (IPIP) [19]. IPIP is a dose planning algorithm that directly optimizes dosimetric indices. It maximizes target coverage and is guaranteed to meet OAR sparing constraints. For this study, dose plans were computed using a prescription dose of 950 cGy, and the source used was Ir-192. Dwell positions were created every 5mm along each needle starting at the tip. Only dwell positions inside the prostate were activated for dose planning. The dose rate parameters were calculated using the point-source formula found in the TG-43 dose calculation protocol [20]. The dose objectives used for this study were the standard dose objectives used at our clinic, and they can be found in the second column of Table I. These dose objectives are based on the recommendations found in the Radiation Therapy Oncology Group (RTOG) 0321 protocol [21]. If the dose plan met the target coverage requirement, and therefore all the requirements, then the needle arrangement was finalized. Otherwise, the δ parameter was adjusted until dose objectives were met by IPIP.

The optimization calculations were carried out using the Matlab interface for CPLEX 12.4, an industrial-grade optimization toolbox by IBM. All calculations were performed on an iMac with a 3.2 GHz Intel Core i5 processor and 16 GB of RAM.

The final planned needle arrangements were labeled P1, P2, P3, and P4, for C1, C2, C3, and C4 respectively. The final number of needles in the arrangements computed for each phantom was 14, 14, 13, and 15, and the target coverage was 95%, 96%, 95%, and 96%, respectively. All other dose constraints were met for the planned arrangements.

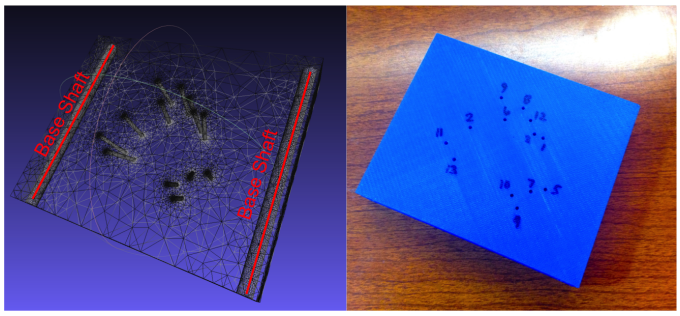

FIG. 4. The guide mesh contained cylindrical channels for each of the needles and two larger base shafts to interface with the base rods (left). We wrote this mesh to a Standard Tesselation Language (STL) file, which is the standard input for 3D printers and 3D printed the needle guides in ABS plastic (right) using a uPrint Plus (Stratasys).

D. Needle Guide Design and Construction

Once a needle arrangement was computed, a triangle mesh was generated for a guide that would produce that arrangement and interface with the base. The surface mesh was generated using in-house software specifically designed for this use-case. The guide was designed to be 12 $\times$10 $\times$ 2 cm with a working area (i.e., space available for needles) of 10 $\times$ 10 cm in the x-y plane, centered on the guide, and the front face of the guide was expected to be 2 cm from the entry face of the phantom. The guide had two circular shafts to interface with the base rods. The shafts were parallel to the y-axis with centers 1 cm from either side on the x-axis, and centered on the guide along the z-axis. Thus the shafts were 11 cm apart, as required by the base. The shafts were designed to be 6 mm in diameter, which is approximately 1 mm more than the measured diameter of the rods. Each needle was intersected with the workspace of the guide and a cylindrical hole, along the direction of the needle, was added to the surface mesh to accommodate it. The holes were created 2 mm in diameter for 1.8 mm diameter needles. The triangle mesh was written to a Surface Tesselation Language (STL) file, which is a standard file format for input to 3D printers.

The guides were printed from the STL files using a uPrint SE Plus (uPrint). The uPrint has a minimum slice resolution of 0.254 mm, which was used for this study, and it has a building volume size of 8 $\times$ 8 $\times$ 6 in. (204 $\times$ 204 $\times$ 152 mm). The guides were printed in ABS plastic, and the support material was an SR-30 soluble material. The guides were

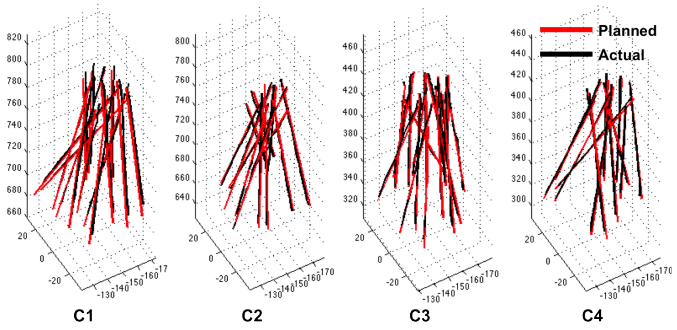

FIG. 5. Planned needle arrangements (red) and actual needle arrangements (black) for each case. The units of the axis are in millimeters. Most of the error is in the z-direction, which is along the needle insertion direction. We expect these errors to be reduced when needles are inserted in the context of a brachytherapy workflow with real-time ultrasound feedback, electromagnetic tracking, and software integration.

printed using the lowest density setting and laid out such that the smallest guide dimension (2 cm) was perpendicular to the printing slices. This layout was used to conserve support material and speed up printing time. The guides each took approximately 4 hours to print, and the support material was dissolved in a lye bath, which took between 4 and 8 hours.

The printed guides fit tightly to the base rods, which did not allow movement between the base and the guide.

E. Needle Insertion

To perform the needle insertion, the phantom and needle guide were placed onto the base. Our experimental setup is shown in Figure 1. A visual interface was designed to assist with the needle insertion step. This interface visually displayed a diagram of the back side of the guide, with needle numbers and insertion depths. The number of each needle was marked on its associated hole. HDR brachytherapy needles were numbered, and rubber stoppers cut from 1/16 in. diameter (1.6 mm) rubber tubes were placed on each needle at the insertion depth specified by the needle insertion interface. The insertion depth was measured from the back of the needle tip. Loading the rubber stoppers onto the needles took less than 10 minutes for each case.

The needles were inserted one at a time up to the stoppers. The needles were twisted

back and forth as they were inserted to facilitate the puncturing of the prostate membrane. There was no ultrasound imaging during needle insertion, and no attempt was made to deviate from the needle arrangement set by the guide. Inserting the needles took less than 5 minutes.

F. Post-processing

Once the needles were inserted, the inner metal stylets of the needles were removed. The phantom, base, guide, and needles were CT scanned. The anatomical structures and needles were segmented in Oncentra. The coordinate systems between the pre- and post-implant scans were registered together using the corner points of the phantom housing. The registration transformation between these two point sets was computed using the Coherent Point Drift Algorithm (CPD) [22]. The actual implanted needle arrangements were labeled A1, A2, A3, and A4, for C1, C2, C3, and C4, respectively. A dose plan was generated using IPIP for each implanted arrangement.

We recorded the volumetric dose distribution and the placement error of the needles for each planned and actual needle arrangement. We also computed a trauma metric that was proposed in Garg et al [12], which is defined as the structure volume displaced by a puncturing needle.

III. RESULTS

The planned and actual needle arrangements for each case are shown in Figure 5. The needles were inserted up to the rubber stoppers at the pre-specified depth. However, some of the needles were pushed out a few millimeters by pressure from the gelatin after they were inserted and had to be pushed back in. The relevant numerical results for this study are shown in Table I. The largest difference in prostate volume between the pre- and post-implant was 6% (2 cm^3). Target coverage and OAR sparing constraints were always met for both the planned and actual arrangements. Target coverage between the planned and actual arrangements were within 2% for every case. The trauma metric is computed by the structure volume displaced by the needle arrangement. This value was computed as the product of the number of penetrated slices, the CT slice thickness, which was 3mm, and the

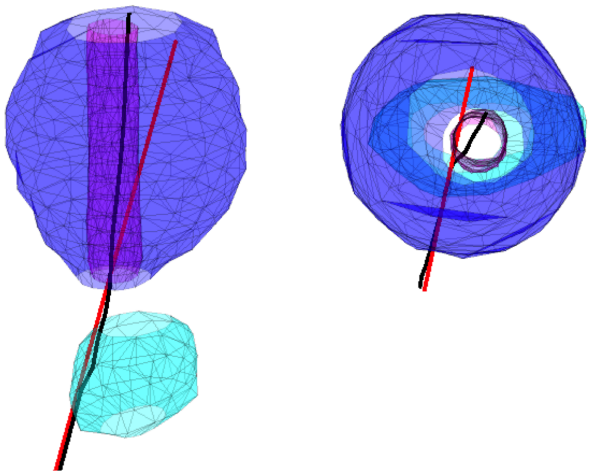

FIG. 6. Failure case for this study. The shown structures are the prostate (blue), urethra (magenta), and penile bulb (cyan). Due to placement error, the planned needle (red) hit the urethra. Since the urethra was modeled by a plastic drinking straw, it could not be punctured (as it would have in a real case) and so the needle turned into the urethra (black).

cross sectional area of the needle, which was conservatively taken to be 1 mm radius. There were three bulb slices punctured in C2, which resulted in a trauma of 28 mm^3. The urethra was also punctured in C2, which is described in more detail in the following paragraph. The trauma metric was 0 for every structure in every other case.

We considered C2 a failure because one needle hit the inside of the bottom of the urethra, and since the urethra was made from a plastic straw, which was not amenable to puncturing, the needle turned in the direction of the urethra and penetrated it throughout its entire length. This failure mode could not happen in a real case because the urethra would been punctured. The same needle also punctured the penile bulb. A diagram of this failure case is shown in Figure 6. The dwell positions in the needle that punctured the urethra in C2 were not included in dose planning.

We used the method in Garg et al [12] to evaluate needle placement error. Points were generated along each planned and actual needle from the tip to 6 cm of its length spaced at 1 mm. The total placement error was computed as the root mean squared error (RMSE) between the corresponding points in the planned and actual arrangements. The total RMSE were 3.6 mm, 3.0 mm, 4.5 mm, and 2.3 mm, respectively. This is larger than the errors reported in Garg et al [12]. The majority of this error is in the z-direction, which is primarily

			C1		C2		C3		C4	
		unit	P1	A1	P2	A2	P3	A3	P4	A4
$V^{Prostate}$		cm^3	27	27	26	28	31	33	32	33
Needles		#	14		14	(13)	13		15	
$V^{Prostate}_{100}$	≥ 90	%	95	94	96	97	95	95	96	94
$V^{Prostate}_{150}$	≤ 45	%	39	38	35	26	39	42	35	36
$V^{Urethra}_{125}$	≤ 0.1	cm^3	0.07	0.07	0.06	0.04	0.08	0.07	0.06	0.08
$V^{Urethra}_{150}$	$= 0$	cm^3	0	0	0	0	0	0	0	0
$V^{Bladder}_{75}$	≤ 1	cm^3	0.16	0	0.48	0.85	0.30	0.52	0.90	0.62
$V^{Bladder}_{100}$	$= 0$	cm^3	0	0	0	0	0	0	0	0
V^{Rectum}_{75}	≤ 1	cm^3	0	0	0	0	0	0	0	0
V^{Rectum}_{100}	$= 0$	cm^3	0	0	0	0	0	0	0	0
V^{Bulb}_{75}	≤ 1	cm^3	0	0	0	0.05	0	0	0	0
V^{Bulb}_{100}	$= 0$	cm^3	0	0	0	0	0	0	0	0
V^{Body}_{100}	$= 0$	cm^3	0	0	0	0	0	0	0	0
T^{Bulb}		mm^3	0	0	0	28	0	0	0	0
$RMSE_x$		mm	0.7	(0.7)	1.4	(1.2)	1.2	(1.1)	0.6	(0.6)
$RMSE_y$		mm	1.2	(0.5)	0.9	(0.9)	0.9	(0.6)	0.7	(0.6)
$RMSE_z$		mm	3.4	(1.8)	2.5	(2.4)	4.2	(2.4)	2.1	(1.7)
RMSE		mm	3.6	(1.9)	3.0	(2.8)	4.5	(2.8)	2.3	(1.9)
$RMSE_{xy}$		mm	1.4		1.7		1.5		0.9	

TABLE I. Dosimetric data, trauma metrics, and needle placement errors for this study. The needle placement errors are reported as the root mean squared error (RMSE) between points generated along each needle in the planned and actual needle arrangement. The RMSE errors are reported in the x-, y-, and z-direction separately, the total distance, and in only the x- and y-direction. Our results showed that most of the error was along the needle insertion direction. In parenthesis are the RMSE after the planned and actual needle arrangements were rigidly registered. Since these errors are still large, registration error is not a likely cause of the total error in our experiment.

along the needle insertion direction and least restricted by the guide. The RMSE between

the planned and actual needles was 1.4 mm, 1.7 mm, 1.5 mm, and 0.9 mm, respectively, when considering only the error in the x- and y-direction. We used CPD to compute the rigid transformation between the planned and actual needle arrangement and the associated errors, which are shown in parenthesis in Table I. The RMSE after the planned and actual arrangements were registered was 1.9 mm, 2.8 mm, 2.8 mm, and 1.9 mm, respectively. The majority of the reduction in RMSE came from an improvement in the z-direction.

IV. DISCUSSION

Our results suggest that skew-line needle guides can achieve high needle insertion accuracy in the x- and y-direction but have large errors in the z-direction. There are two likely causes for high error in the z-direction. Since the needle insertion direction is primarily in the z-direction, the errors in the z-direction could be caused by uncertainty in needle insertion depth due to reinserting the needles, or the error could be caused by uncertainty in finding the needle tip during segmentation, since the scans were taken in 3 mm slices in the z-direction. The needle placement errors are not likely caused by errors in registration since performing a least-squares transformation between the planned and actual needle arrangements did not eliminate the majority of the error.

The needle placement errors resulted in one failure case. Although in practice this case would have been catastrophic, the custom needle guides explored in this study are expected to be used in the context of a system that includes real-time ultrasound feedback and EM tracking, which would allow the user to abort the needle if it was about to puncture an OAR. Needle guides could be populated with redundant channels that could be used as alternatives in this case. The ultrasound and EM tracking could also potentially reduce the overall placement errors found in this study.

Currently the vast majority of the workflow time is spent in printing the needle guides. However, it is possible that 3D printing speed will improve as the technology continues to develop. It is also possible to produce the needle guides using a 5-axis CNC drill. However for this study, we did not have access to a CNC drill, and it is reasonable to assume that hospitals will be equipped with 3D printers in the future given the amount of work in medical applications of 3D printing [23], including in brachytherapy [24].

V. CONCLUSION

We evaluated the needle placement errors associated with using custom, skew-line needle guides for prostate HDR brachytherapy. The placement errors in the x- and y-direction were small, but there were substantial errors in the z-direction. This error did not affect the ability to meet treatment dose objectives. To reduce errors, future work should evaluate the use of custom needle guides in the context of a system that includes real time ultrasound, EM tracking, and novel optimization techniques.

VI. ACKNOWLEDGEMENTS

We thank Sarah Geneser, Atchar Sudhyadhom, and the clinical staff in the Department of Radiation Oncology at UCSF for helping execute the experimental workflow. We thank Professor Paul Wright at UC Berkeley for generously giving us access to 3D printers.

---

[1] K. Wallner, J. C. Blasko, and M. Dattoli, *Prostate brachytherapy made complicated*. SmartMedicine Press, 2001.

[2] A. Sabbas, F. Kulidzhanov, J. Presser, M. Hayes, and D. Nori, "HDR brachytherapy with surface applicators: technical considerations and dosimetry." *Technology in Cancer Research & Treatment*, vol. 3, no. 3, p. 259, 2004.

[3] P. W. Grigsby, "Vaginal cancer," *Current Treatment Options in Oncology*, vol. 3, no. 2, pp. 125–130, 2002.

[4] M. Keisch, F. Vicini, R. R. Kuske, M. Hebert, J. White, C. Quiet, D. Arthur, T. Scroggins, and O. Streeter, "Initial clinical experience with the mammosite breast brachytherapy applicator in women with early-stage breast cancer treated with breast-conserving therapy," *International Journal of Radiation Oncology* Biology* Physics*, vol. 55, no. 2, pp. 289–293, 2003.

[5] A. N. Viswanathan, J. Dimopoulos, C. Kirisits, D. Berger, and R. Pötter, "Computed tomography versus magnetic resonance imaging-based contouring in cervical cancer brachytherapy: results of a prospective trial and preliminary guidelines for standardized contours," *International Journal of Radiation Oncology* Biology* Physics*, vol. 68, no. 2, pp. 491–498, 2007.

[6] J. N. Roy, K. E. Wallner, P. J. Harrington, C. C. Ling, and L. L. Anderson, "A CT-based evaluation method for permanent implants: application to prostate," *International Journal of Radiation Oncology* Biology* Physics*, vol. 26, no. 1, pp. 163–169, 1993.

[7] Y. Kim, I.-C. J. Hsu, and J. Pouliot, "Measurement of cranio-caudal catheter displacement between fractions in CT-based HDR brachytherapy of prostate cancer," *Journal of Applied Clinical Medical Physics*, vol. 8, no. 4, 2007.

[8] W. Foster, L. Beaulieu, F. Harel, A. Martin, and E. Vigneault, "The impact of 3D image guided prostate brachytherapy on therapeutic ratio: the Quebec University Hospital experience," *Cancer radiotherapie: journal de la Societe francaise de radiotherapie oncologique*, vol. 11, no. 8, pp. 452–460, 2007.

[9] J. Cunha, I. Hsu, and J. Pouliot, "Dosimetric equivalence of nonstandard HDR brachytherapy catheter patterns," *Medical Physics*, vol. 36, no. 1, pp. 233–239, 2008.

[10] J. Xu, V. Duindam, R. Alterovitz, J. Pouliot, J. A. M. Cunha, I.-C. Hsu, and K. Goldberg, "Planning fireworks trajectories for steerable medical needles to reduce patient trauma," in *Intelligent Robots and Systems, 2009. IROS 2009. IEEE/RSJ, International Conference on.* IEEE, 2009, pp. 4517–4522.

[11] T. Siauw, A. Cunha, D. Berenson, A. Atamtürk, I.-C. Hsu, K. Goldberg, and J. Pouliot, "NPIP: A skew line needle configuration optimization system for HDR brachytherapy," *Medical Physics*, vol. 39, no. 7, pp. 4339–4346, 2012.

[12] A. Garg, T. Siauw, D. Berenson, J. A. M. Cunha, I.-C. Hsu, J. Pouliot, D. Stoianovici, and K. Goldberg, "Robot-Guided Open-Loop Insertion of Skew-Line Needle Arrangements for High Dose Rate Brachytherapy," *Transactions on Automation Science and Engineering*, vol. 10, no. 4, pp. 948–956, 2013.

[13] M. Baumann, P. Mozer, V. Daanen, and J. Troccaz, "Towards 3D ultrasound image based soft tissue tracking: a transrectal ultrasound prostate image alignment system," in *Medical Image Computing and Computer-Assisted Intervention–MICCAI 2007.* Springer, 2007, pp. 26–33.

[14] D. Cool, S. Sherebrin, J. Izawa, J. Chin, and A. Fenster, "Design and evaluation of a 3D transrectal ultrasound prostate biopsy system," *Medical physics*, vol. 35, no. 10, pp. 4695–4707, 2008.

[15] A. Jain, L. Gutierrez, and D. Stanton, "3D TEE registration with X-ray fluoroscopy for interventional cardiac applications," in *Functional Imaging and Modeling of the Heart*. Springer, 2009, pp. 321–329.

[16] Z. Yaniv, E. Wilson, D. Lindisch, and K. Cleary, "Electromagnetic tracking in the clinical environment," *Medical Physics*, vol. 36, no. 3, pp. 876–892, 2009.

[17] A. Karabis, P. Belotti, and D. Baltas, "Optimization of catheter position and dwell time in prostate HDR brachytherapy using HIPO and linear programming," in *World Congress on Medical Physics and Biomedical Engineering, September 7-12, 2009, Munich, Germany*. Springer, 2009, pp. 612–615.

[18] E. Poulin, C.-A. C. Fekete, M. Létourneau, A. Fenster, J. Pouliot, and L. Beaulieu, "Adaptation of the CVT algorithm for catheter optimization in high dose rate brachytherapy," *Medical Physics*, vol. 40, no. 11, p. 111724, 2013.

[19] T. Siauw, A. Cunha, A. Atamtürk, I.-C. Hsu, J. Pouliot, and K. Goldberg, "IPIP: A new approach to inverse planning for HDR brachytherapy by directly optimizing dosimetric indices," *Medical Physics*, vol. 38, no. 7, pp. 4045–4051, 2011.

[20] M. J. Rivard, B. M. Coursey, L. A. DeWerd, W. F. Hanson, M. S. Huq, G. S. Ibbott, M. G. Mitch, R. Nath, and J. F. Williamson, "Update of AAPM Task Group No. 43 Report: A revised AAPM protocol for brachytherapy dose calculations," *Medical Physics*, vol. 31, no. 3, pp. 633–674, 2004.

[21] I. Hsu, K. Bae, K. Shinohara, J. Pouliot, J. Purdy, G. Ibbott, J. Speight, E. Vigneault, R. Ivker, H. Sandler *et al.*, "Phase II trial of combined high-dose-rate brachytherapy and external beam radiotherapy for adenocarcinoma of the prostate: preliminary results of RTOG 0321," *International Journal of Radiation Oncology* Biology* Physics*, vol. 78, no. 3, pp. 751–758, 2010.

[22] A. Myronenko and X. Song, "Point set registration: Coherent point drift," *Pattern Analysis and Machine Intelligence, IEEE Transactions on*, vol. 32, no. 12, pp. 2262–2275, 2010.

[23] F. Rengier, A. Mehndiratta, H. von Tengg-Kobligk, C. Zechmann, R. Unterhinninghofen, H.-U. Kauczor, and F. Giesel, "3d printing based on imaging data: review of medical applications," *International Journal of Computer Assisted Radiology and Surgery*, vol. 5, no. 4, pp. 335–341, 2010.

[24] C. Zemnick, S. A. Woodhouse, R. M. Gewanter, M. Raphael, and J. D. Piro, "Rapid prototyping technique for creating a radiation shield," *The Journal of Prosthetic Dentistry*, vol. 97, no. 4, pp. 236–241, 2007.